University of Sistan and Baluchestan

Journal of Epigenetics

Online ISSN: 2676 - 4350

Homepage: https://jep.usb.ac.ir

Iranian Genetics Society

New Piperidin-4-Amine Derivatives as Anti-HCV Inhibitors: A Structure-Based Approach Combining DFT, QSAR, and ADMET Analysis Targeting NS5B Polymerase

Abubakar Sadiq Bello [1*], Adamu Uzairu[2], Shallangwa Gideon .Adamu[3], Abdulkadir Ibrahim [4], Muhammad Tukur Ibrahim[5]

[1] *Corresponding author*, Department of Chemistry, Faculty of Physical Science, Ahmadu Bello University, P.M.B 1045, Zaria, Kaduna State, Nigeria E-mail: sadiqbello@afit.edu.ng

[2,3,4,5] Department of Chemistry, Faculty of Science, Air force Institute of Technology, P.M.B 2104, Kaduna State, Nigeria.. E-mail: adamuuzairu@gmail.com, gashallangwa@gamial.com, ibrahimabdulkadir@gmail.com, mtibrahim@abu.edu.ng

ARTICLE INFO

Article type:
Research Article

Article history:
Received:27 February 2025
Revised:9 April 2025
Accepted:1 May 2025

Keywords:
Hepatitis C,
NS-5B Polymerase,
ADMET properties,
Molecular docking,
QSAR,
Molecular Design,
Pharmacokinetics.

A B S T R A C T

Hepatitis C virus (HCV) is a major cause of severe liver disease, leading to complications such as cirrhosis, liver failure, and hepatocellular carcinoma, liver damage, and basic cancer of the liver (hepatocellular carcinoma). There have been major therapeutic advances since the virus's discovery. Recent research has shown that plant-derived compounds are increasingly valuable in the development of innovative, effective, and cost-effective anti-Hepatitis C Virus treatments. In the current work, a complete examination of 31 piperidin derivatives was performed, these molecules were computationally examined using a through in-silico technique that includes 2D-3D Quantitative Structure Activity Relationship (QSAR) simulation and docking of molecular structures, and their properties were confirmed using ADMET and Density Functional Theory (DFT) calculations. The anti-hepatitis C compounds have been optimized utilizing the DFT approach using the B3LYP version and 6-31G* basis set. The Genetic Function Algorithm (GFA) was utilized to develop five models. An externally verified test set, Y-randomization, variance inflation factor (VIF), mean effect (MF), and William's plot applicability domain (AD) were used to build and validate a credible 2D QSAR model (R2 internal = 0.8537, R2 external = 0.6979). Compound 26 was the most promising candidate because of its remarkable binding affinity, which was demonstrated by the high molecular docking score of -142.24 kcal/mol that was obtained from the virtual screening of the compounds under investigation. A structure-based approach created six new molecules with increased affinity for the NS5B polymerase (SCD6 -153.74 kcal/mol). The newly discovered compounds have higher mole dock ratings than the FDA medicine Rib/Pig (-111.095 kcal/mol). According to the predicted drug-likeness and ADMET features, the most recently found compounds have a bioavailability value of 0.17, are easily synthesized in the wet laboratory (based on the synthetic accessibility value), and have favorable pharmacokinetic profiles. The developed molecule SCD6, which is stable, has greater affinity, and has the best pharmacokinetic features, should be produced in the wet lab as prospective Hepatitis C viral agents.

Introduction

Hepatitis C virus (HCV) is a single-stranded RNA virus (~9.6 kb) belonging to the Flaviviridae family. It replicates using NS5B RNA-dependent RNA polymerase, making this enzyme a crucial antiviral drug target (1). Hepatitis C virus (HCV) is the most prevalent cause of persistent liver disease worldwide, including catastrophic consequences including cirrhosis, liver damage, and primary liver cancer (hepatocellular carcinoma). The acute infection is typically unaffected by symptoms which, in addition to

DOI: https://doi.org/ 10.22111/JEP.2025.51275.1081

© The author(s) **Publisher**: University of Sistan and Baluchestan

How to Cite: Sadiq Bello, A., Uzairu, A., Gideon .Adamu, Sh., Ibrahim, A., & Ibrahim, M.T. (2025). New Piperidin-4-Amine Derivatives as Anti-HCV Inhibitors: A Structure-Based Approach Combining DFT, QSAR, and ADMET Analysis Targeting NS5B Polymerase. *Journal of Epigenetics*, 6(1), 47-63. https://doi.org/ 10.22111/JEP.2025.51275.1081

inadequate awareness and demographic screening, results in severe liver disease when discovered. According to WHO estimates, HCV infection caused over 400 000 deaths in 2015, with over 1.75 million new infections per year. New direct-acting antivirals (DAA) have changed HCV antiviral therapy, which was formerly based on recombinant type one interferon (IFN) and the guano sine analogue ribavirin (2). DAA constitutes an exceptional therapeutic development feat, with the ability to provide large cure rates with favorable safety characteristics, allowing its use in patients with severe illnesses (3). DAA is currently targeting three amino acids inside the replication process of the virus (NS3/4A protease, NS5A, and the NS5B RNA-dependent RNA polymerase (RdRP), having various combinations of drugs accessible for use against every one of the eight viral types (1).

Nevertheless, the absence of a human HCV vaccine or similar prophylactic renders DAA-based reduction attempts for approximately 71 million of the persistently contracted individuals highly challenging. DAA accessibility remains restricted due to expenses, which correlates to low diagnoses and a growing prevalence in nations with low or middle incomes (LMIC). Persistent viruses pose a growing problem (4), recent findings of increasing resistance among some uncommon virus strains (4).

Compliance among patients with elevated risk is low, and effective DAA treatment fails to avoid another infection. Furthermore, current research suggests that DAA may be less effective in reducing the possibility of HCC in treating individuals than IFN-based therapy (5). It might be connected to virus-induced human epigenetic markers which cannot be eliminated following DAA treatment (6, 7). As a result, new pharmaceutical techniques with more efficacy and fewer side effects must be sought for. Structure-based drug discovery and design is one of the most extensively used methodologies among medicinal chemists.

Structure-based drug design, particularly QSAR and molecular docking, has emerged as a powerful approach for predicting compound efficacy before synthesis. The widely recognized quantitative structure-activity relationships (QSAR) approaches include part of the structure-based technique (8), (9), This depends on modifications to the structural characteristics of compounds, such as steric, electrostatic in nature, and hydrophobic. QSAR approaches are being utilized to identify important structural properties that contribute to medicines' anti-hepatitis C activity (10, 11). QSAR is a significant aspect in drug design; consequently, it is rather obvious that many users of QSAR are located largely in the research divisions of enterprises (9, 12). As a result, before synthesizing the planned leads, a QSAR model must be built to forecast their activity. An effective QSAR modeling not only aids in the identification of connections among the chemical structure and biological functions of any kind of compound, but it also provides scholars with a complete study of the most important compounds for use in subsequent investigations (10). Additionally, knowing the mechanism of ligand/receptor interactions is critical for drug development, as molecular docking modeling is an effective method for acquiring this knowledge. Molecular docking modeling is a computer technique used to estimate the capacity for binding residues in the active site to specific molecules on the receptor and to disclose the magnitude of the interaction (13). Docking is a very effective and extensively used approach in drug development to analyze the binding of tiny molecules (inhibitors) with receptors (macromolecules) (14) (15). The goal of the research aimed to develop novel strong compounds on the N-phenethylpiperidin-4-amine by QSAR modeling accompanied by a Molecular Docking modeling utilizing the compounds acquired during the research (16).

If we want a treatment to be effective, we must balance its toxicity, pharmacokinetics, and potency. During pre-clinical trials, it is necessary to identify acceptable features for drug adsorption, distribution, metabolism, excretion, and toxicity (ADMET) (17). As a vital component of the drug development process, ADMET investigations have been carried through by undertaking drug metabolism and pharmacokinetics (DMPK) research (18). These investigations assist in determining the practicality of a medicine option utilizing knowledge gathered through ADMET properties/data (18, 19). Immediate ADMET characterization of a treatment potential within preclinical trials can reduce the likelihood of going into clinical trials. Because pharmaceutical manufacturing failures are driven by potency or safety issues, preliminary ADMET assessment of a therapeutic concept is essential to uncover drugs

with potency and those with substantial limitations (20).

DFT and Time-Dependent DFT (TDDFT) constitute two of the many commonly utilized methodologies for investigating structural characteristics, spectral properties, and other geometries that depend on organic molecules' structural characteristics. B3LYP is a hybrid function for organic molecules (21) remains the most popular method because it is less computationally expensive than alternative Post-Hartree-Fock approaches and achieves equivalent outcomes. The LUMO determines the molecule's capability to seize electrons, whereas the HOMO reveals the molecule's capacity to give away electrons. The HOMO-LUMO energy gap (DE) represents the variation in the energy levels among the Highest Occupied Molecular Orbital (EH) and Lowest Unoccupied Molecular Orbital (EL) orbitals, which describes the following charge exchange relationship that happens throughout the molecule. (22).

Materials and Techniques

QSAR Modeling Methodology

Data Source

Adam Rolt with collaborators developed thirty one (31) piperidin-4-amine chemical derivatives and investigated their effects against the hepatitis C virus (HCV) (16). It only presented the 50% inhibitory dose (EC50) of piperidine-4-amine compounds towards hepatitis C virus (µm). Equation (1) was then used to convert/transform the activities into their respective logarithmic scales.

$$pEC_{50} = \frac{-\log EC50}{10^{-6}} \quad \text{..... (1)}$$

Tables

Table 1 includes associated information for each ligand, such as the molecular formula, pEC50 values, and residual values.

Table 1- shows the actual and anticipated pEC50 (µm) of piperidin derivatives against NS5B polymerase.

S/N	Molecular Formula	Actual values pEC50(µm)	Predicted values pEC50 (µm)	Residual values pEC50(µm)
1X	N-phenethyl-N-(2-propylcyclopentyl)piperidin-4-amine	5.9355	5.9115	-0.0240
2	N-phenethyl-N-(2-propylcyclohexyl)piperidin-4-amine	5.8632	5.8302	0.0330
3	N-phenethyl-N-(2-(prop-1-en-1-yl)phenyl)piperidin-4-amine	5.8297	5.7298	0.0999
4	N-(2-allylphenyl)-N-phenethylpiperidin-4-amine	5.5497	5.7097	-0.1599
5	1-(2-(phenethyl(piperidin-4-yl)amino)phenyl)propan-1-one	5.5086	5.6315	-0.1229
6	N-(4-chloro-3-fluorobenzyl)-N-phenethylpiperidin-4-amine	5.4001	5.6106	-0.2105
7	N-(3-fluorobenzyl)-N-phenethylpiperidin-4-amine	5.4156	5.3693	0.0462
8	N-benzyl-N-phenethylpiperidin-4-amine	5.6777	5.6587	0.0190
9	N-(4-chlorobenzyl)-N-phenethylpiperidin-4-amine	5.8664	5.8556	0.0108
10	N-(4-bromobenzyl)-N-phenethylpiperidin-4-amine	5.7878	5.8082	-0.0204
11	N-(4-fluorobenzyl)-N-phenethylpiperidin-4-amine	6.0362	6.1138	-0.0776
12	N-phenethyl-N-(4-(trifluoromethyl)benzyl)piperidin-4-amine	5.9746	5.9525	0.0221
13	N-phenethyl-N-(4-(trifluoromethoxy)benzyl)piperidin-4-amine	5.8894	5.6956	0.1937
14X	N-(4-methoxybenzyl)-N-phenethylpiperidin-4-amine	5.6055	5.4382	-0.1673
15	N-(4-methoxybenzyl)-N-phenethylpiperidin-4-amine	5.4111	5.4168	-0.0056
16	4-((phenethyl(piperidin-4-yl)amino)methyl)benzonitrile	5.1307	5.1483	-0.0175
17X	N-(3-chlorobenzyl)-N-phenethylpiperidin-4-amine	6.3467	5.9448	-0.4019
18	N-(3-bromobenzyl)-N-phenethylpiperidin-4-amine	6.0132	5.8851	0.1281
19	N-(3-fluorobenzyl)-N-phenethylpiperidin-4-amine	5.9172	5.9096	0.0075
20	N-phenethyl-N-(3-(trifluoromethyl)benzyl)piperidin-4-amine	5.7447	5.6546	0.0900
21	N-phenethyl-N-(3-(trifluoromethoxy)benzyl)piperidin-4-amine	5.4259	5.4669	-0.0409
22	N-(3-methylbenzyl)-N-phenethylpiperidin-4-amine	5.4365	5.5780	-0.1415
23	3-((phenethyl(piperidin-4-yl)amino)methyl)phenyl hypochlorite	5.8538	5.6652	0.1886

24	3-((phenethyl(piperidin-4-yl)amino)methyl)phenyl hypobromite	5.6595	5.7470	-0.0875
25	3-((phenethyl(piperidin-4-yl)amino)methyl)phenyl hypofluorite	5.2823	5.5070	-0.2247
26	N-phenethyl-N-(3-(trifluoromethoxy)benzyl)piperidin-4-amine	5.5850	5.4815	0.1034
27	N-(3-(methylperoxy)benzyl)-N-phenethylpiperidin-4-amine	5.7569	5.5131	0.2438
28 X	N-(3,5-dichlorobenzyl)-N-phenethylpiperidin-4-amine	6.3187	5.8892	-0.4295
29	N-(3-bromo-4-chlorobenzyl)-N-phenethylpiperidin-4-amine	6.6777	6.6760	0.0016
30 X	N-(4-chloro-3-fluorobenzyl)-N-phenethylpiperidin-4-amine	5.9625	5.9506	-0.0119
31	N-(4-chloro-3-fluorobenzyl)-N-phenethylpiperidin-4-amine	5.8041	5.8829	-0.0788

X = test set

Generate and optimize structures.

ChemDraw ultra-software edition 12.0 generated 2D structures of piperidine-4-amine compounds. Spartan 14 software has been employed to turn these 2D structures into 3D structures and conduct an equilibrium geometry search (23). The resulting equilibrium geometrical composition having minimal energy adheres to the composition and characteristics of the chemical as they occur naturally (24). The optimal geometry with the lowest energy was calculated via DFT and the 6-31G* basis set. These improved geometries were saved to a protein database (pdb) kind of document (25).

Molecular descriptors, data preprocessing, and division

The Pharmaceutical Data Exploration Laboratory's (PaDEL) descriptors toolkit has been employed to create independent variables (molecular descriptors) for all calculated structures with the lowest energy. The PaDEL software package produced different descriptors (one-dimensional, two-dimensional, and three-dimensional) (25). The generated data was processed with data pretreatment software to remove insufficient data, redundant operation, and consistent descriptors (26). The Kennard Stone algorithm was used to divide the treated data into a training and test set, with the training set being 80% and the test set comprising 20% (27). The models were generated using the training data, and they were validated and assessed using the test set.

Validating the Model

Internal validation of the models was conducted using a variety of statistical techniques, including coefficient of determination (R^2), adjusted coefficient of determination (R^2 adj), cross-validation coefficient (Q^2cv), and other validation methods and approaches. Equation (2) describes the mathematical calculations. $R^2 = 1 - \frac{\Sigma (Y_{obs} - Y_{pred})^2}{\Sigma (Y_{obs} - \bar{y}_{training})^2}$ ……. (2)

For Equation (2), Ypred, Yobs, and Ym/trn represent the training set's expected, experimental, and mean experimental activity, respectively. Further to the coefficient of correlation R^2, the adjusted coefficient of determination R^2 adj was determined to confirm the reliability of a model, as indicated in Equation (3).

$$R^2_{adj} = 1 - (1-R^2) \frac{N-1}{N-P-1} = \frac{(N-1)\,R2-P}{N-P+1}$$ …… (3)

Equation (3) identifies P as the number of descriptors in the mathematical model, whereas n represents the total number of compounds in the training set. Q2cv used cross-validation using the single leave-out Equation (4) to estimate the predictive capability of the models.

$$Q^2_{cv} = 1 - \frac{\Sigma(Ypred-Yexp)^2}{\Sigma (Yexp-Ymtraining)^2} \quad \ldots\ldots\ldots (4)$$

Equation (4) represents the training set's anticipated, experimental, and mean experimental activities as Ypred, Yexp, and Ym/trn. For external validation, we confirmed the resilience and predictive capability of a model's coefficient of determination, which was determined using the test set and Equation (5).

$R^2_{pred} = 1 - \Sigma (Y_{pred} - Y_{exp}) / \Sigma (Y_{exp} - Y_{mntrng})$ ……. (5)

In Equation (5), Ypred, Yexp, and Ym/tst indicate the test set anticipated, experimental, and mean experimental activity, respectively.

Evaluation of multi-co-linearity, mean effect, and randomization test

The Y-randomization test is yet another significant validating tool for determining a QSAR model's resilience. This is accomplished by modifying the

variables that are reliant relative to the unadjusted distinct independent variables. The experiment was carried out on a training set, and the generated R^2 and Q^2 values were expected to be lower compared to the observed R^2 and Q^2, demonstrating that the predictive model is dependable and robust rather than based on random association. The CR2 p has been calculated as well and is expected to be greater than or equal to 0.515 (Muhammad *et al.*, 2018), Equation 6 depicts the formula. $cR^2p = R \times (R^2 - R^2r)^2$…….. (6).

Equation (6) defines CR^2p as The factor of dependence for Y-randomization, R as the Y-randomization correlation coefficient, and Rr as the average 'R' of random models. Equation (7) determines each descriptor's effective involvement and contribution to a particular model, frequently referred to as the mean effect.

$$M_J = \frac{\left(\beta_J \sum_{i=1}^{i=n} d_{ij}\right)}{b\left(\sum_j^m \beta_j \sum_1^n d_{ij}\right)} \quad (7)$$

In Equation (7), MEj symbolizes the average impact of the descriptor j; bj represents the coefficient of the descriptor j; dij symbolizes the average effect for every compound's chosen descriptors; m symbolizes the number of descriptors in a produced model; n symbolizes the total number of compounds in the training set. The predicted ME value reveals the magnitude and direction of every descriptor's involvement in an algorithm of compounds comprising the training dataset (Abdullahi *et al.*, 2020). To discover multi-colinearity among model descriptors, we determined the VIF for each and every one. This demonstrated how closely the descriptions correlated with one another. When the variance inflation factor value is equal to 1, there is often no relationship between one descriptor and another; when it varies from 1 to 5, there is a likelihood of adopting the model; whereas if it surpasses 10, the model must be disregarded since one descriptor is highly related to the other (Olasupo *et al.*, 2019), VIF was computed using Equation (8).

$$VIF = \frac{1}{R_{ij}^2} \quad \text{…….. (8)}$$

In Equation (8), VIF denotes a descriptor's variance inflation factor, and R^2ij indicates The relationship coefficient of a multiple analysis among descriptor i and the remainder j in the generated model.

The produced model's applicable domain

The applicability domain (AD) is a conceptual area inside the chemical environment. This represents William's lot showing standardized residual values (variations among expected and actual activities) with compound leverage values for a particular data set.AD computes the leverage value of a novel chemical to assess whether it belongs within the applicability domain and detects outliers or influencer molecules (Olasupo *et al.*, 2019). Equation (9) was used to obtain the leverage value hi for a specific molecule.

$$hi = X^i (X^T X)^{-K} X^iT \quad (i = A,\ldots, Z) \quad \text{…….(9)}$$

Equation (9), where Xi is the training set compound matrix, X is the n × k descriptor matrix of the training set compound, and XT is the transpose matrix of X utilized to create the model. Equation (10) determines the point of threshold or warning leverage number.

$$h^* = 3(p + 1)/n \quad \text{…….(10)}$$

In Equation (10), n and p denote the number of training compounds and descriptors utilized in a model.

DFT computations

To investigate the structural geometry, we performed DFT/B3LYP level simulations on the studied substances. In conjunction with geometry optimization, evaluating the frontier molecular orbitals is a useful tool for determining molecule reactivity and investigating electron stimulation spanning the HOMO to the molecular orbital that is least occupied (LUMO). The LUMO determines the capacity of a molecule to seize an electron, while the HOMO reveals its capacity to give away one. The HOMO-LUMO energy gap (DE) is the distinction in energy levels that exist between HOMO (EH) and LUMO (EL) orbitals, which are responsible for the subsequent charge transfer interactions inside the molecule. We may use the energy gap (DE) to determine the kinetic and physical responses for these compounds. In actuality, molecules that have a small energy gap are characterized by high chemical reactivity and low kinetic stability and are referred to be flexible molecules. Hard molecules, on the other hand, are more stable due to their large energy gap. This is owing to their hostility to charge transfer and changes in electron density and dispersion (Fukui, 1982). Furthermore, certain other properties may be utilized to characterize a greater number of the molecules that are strongly connected with the HOMO and LUMO forces,

including the ionization potential (IP = -EH) and the affinity of electrons (EA = -EL) (Wolinski et al., 1990). Using these properties, we can compute the following (Gázquez, 1993)

The formula for global hardness (η) (and its inverse, σ global softness) indicates a molecule's polarizability.

$$\eta = \frac{IP-EA}{2} \quad \text{.....11}$$

Electronegativity (□) refers to a molecule's ability to draw in electrons, as illustrated by the following method:

$$\square = \frac{IP+EA}{2} \quad \text{.....12}$$

Chemical potential (μ) is the initial derivative of the overall energy based on the quantity of electrons in a molecule. It symbolizes an electron's tendency to depart (El Kalai et al., 2019). Chemical potential is just the inverse of electronegativity:

$$\mu = -\square \quad \text{.....13}$$

The Electrophilicity index (ω) is a measure of a substance's ability to take electrons and was proposed to assess its electrophilic power. The formula states:

$$\omega = \frac{\mu^2}{2\eta} \quad \text{.....14}$$

Table 6 lists the computed proprieties. These findings indicate a significant difference in EH, EL, and DE.

Methodology for Molecular Docking

The receptor's crystalline structure was obtained from https://www.rcsb.org with its protein data bank (pdb) registration ID 3FQK. Molegro's virtual Docker software 2013 version 6.0.1 was used to view the receptor (Cui *et al.*, 2020). The NS5B polymerase was imported into the Molegro virtual Docker and updated the hydrogen atoms, deleted unnecessary water molecules, assigned bonds (if necessary), created explicit hydrogen, assigned charges, and detected flexible torsion in ligands discovered in the X-ray structure. All of the generated compounds (piperidin-4-amine) were Uploaded in Molegro Virtual Docker 6.0, Docking wizard with PLANTS score (Grid) at a resolution of A° (0.30), together with NS5B polymerase (reference inhibitor), for molecular docking with a radius of 20 at that time. The amino acid side chains, which were likewise inserted inside the confined sphere, were linked together using the bond flexibility (Abdullahi *et al.*, 2020). The flexibility was set to 0.90 with a 1.10 tolerance. Considering numerous cluster postures with 100.00 energy penalty levels, an RMSD threshold of 2.00 A was adopted. The docking mechanism was set up for a maximum of 1500 repetitions and a simplex evolution size of 50 (Abdullahi *et al.*, 2020). Each of the 20 postures was docked at least 50 times, and the best poses were chosen using predetermined scoring standards such MolDock, Rerank, plant, and heavy atoms (Thomsen and Christensen, 2006). The Discovery Studio (DS) Visualizer v. 3.5 displayed a variety of intermolecular interactions, including H-bonds, hydrophobic, halo-bonds, and aryl contacts (Nulamuga *et al.*, 2023).

ADME characteristics and prediction of drug-likeness

SwissADME, a free online tool for evaluating small compounds' drug-likeness and ADME characteristics, certain selected anti-hepatitis C drugs from the data set had their ADME properties and drug-likeness predicted. A chemical is considered to be violating Lipinski's rule of five if it exceeds two of the following criteria: molecular weight < 500, number of hydrogen bond donors ≤ 5, number of hydrogen bond acceptors ≤ 10, calculated log p ≤ 5, and polar surface area (PSA) < 140 $\overline{2}$, According to some, the chemical is beneficial during the pre-clinical phase of drug discovery and is either impermeable or poorly absorbed (Bello *et al.*, 2024).

Designing new chemicals

To increase drug resemblance, novel compounds were designed by augmenting and strengthening the affinity of piperidin-4-amine analogs for the receptor. Compounds 26 and 30 were chosen because they had better MolDock, Rerank, plant, and heavy atoms scores against NS5B polymerase (-142.24 and 140.70, respectively, as shown in Table 7). This was accomplished by subtly manipulating these two compounds, either by adding, deleting, or substituting their substituents using bioisosterism knowledge. This resulted in the development of six new chemicals. SWISSADME, a free online web tool (http://www.swissadme.ch/index.php), and

pkCSM, an online web server (http://structure.bioc.cam.ac.uk/pkcsm), have been utilized to determine the pharmacokinetics, drug-likeness, and medicinal chemistry associated with those compounds (Ismail and Uzairu, 2019).

Findings and Discussion

Quantitative SAR model

The QSAR model was developed with biological activity as the reaction or dependent variable and chemical descriptors as the independent variable. This QSAR model quantitatively correlates piperidin-4-amine's action to its chemical structure, laying the groundwork to forecast the biological response of a new medication in the same chemical region.

Developing QSAR models

The QSAR model has been created using Material Studio software and the Genetic Algorithm/Multiple Linear Regression method. Five models were generated with the data set, and the most successful model was chosen based on a high squared correlation coefficient R^2 (0.8507), a low residual, and a high coefficient of prediction for the test set, R^2 test set (0.7821).

The preferred model is depicted in equation (15). Table 1 shows the predicted pEC_{50} value and residual values from the data set produced by the suggested computational framework.

Model 5. pEC50 = 0.212557355 * AATS3i + 8.022250576 * SpMax2_Bhm - 0.020507511 * TopoPSA + 6.317442424 * E3i - 8.577744073 * E3s -57.53083307. …….(15)

The evaluation test results demonstrated that the QSAR model was efficient, reputable, and predictive. This resulted in a robust and effective predictive model satisfying the validation tests in Table 2.

Table 2- shows the validation parameters of the models developed using the values that were suggested for evaluating a valid QSAR model.

Parameters	Model 1	Model 2	Model 3	Model 4	Model 5
Friedman LOF	0.0808	0.0811	0.0812	0.082368	0.0824
R-squared	0.8537	0.8531	0.8530	0.85093	0.8507
Adjusted R-squared	0.8171	0.8164	0.8162	0.813663	0.8134
Cross validated R-squared	0.7686	0.7466	0.7428	0.77495	0.7671
Significant Regression	Yes	Yes	Yes	Yes	Yes
Critical SOR F-value (95%)	2.7329	2.7329	2.7329	2.732939	2.7329
Lack-of-fit points	20	20	20	20	20
Min expt. error for non-significant LOF (95%)	0.1058	0.1061	0.1061	0.106901	0.106
External Validation	0.6979	0.6570	0.6863	0.7650	0.7821

The model has the following 2-D and 3-D descriptors: Table 3 shows the Centered Broto-Moreau autocorrelation - lag 3/weighted by Sanderson electro negativities (AATS3i), the largest absolute eigenvalue of the Burden modified matrix—n 2 / weighted by relative first ionization potential (SpMax2_Bhm), the topological polar surface area (TopoPSA), and the component accessibility directional WHIM index / weighted by I-state (E3).

Table 3- Specification of entered descriptors, their class and symbols.

Symbol	Description	Class
AATS3i	Centered Broto-Moreau autocorrelation - lag 3/weighted by Sanderson electro negativities	2D
SpMax2_Bhm	Largest absolute eigenvalue of Burden modified matrix—n 2 / weighted by relative first ionization potential	2D
TopoPSA	Topological polar surface area	2D
E3s	component accessibility directional WHIM index / weighted by I-state	2D

The findings of the Y-randomization test suggest the model is not dependent on opportunity affiliation. The smaller aggregate randomization principles of R^2 and Q^2 in Table 4 are shown below. Furthermore, the cRp^2 score exceeded 0.5. The descriptors indicated no multi-co-linearity, and the VIF value in Table 5 fell within acceptable limits. The following suggested that the developed model was acceptable. The remaining column of Table 5 shows the operational role of all descriptors, also known as the mean effect ME. This highlights the involvement of all descriptors in influencing reaction activity; a negative value

indicates a descriptor has an undesirable effect (the presence of the descriptor reduces activity, while its absence increases activity). A positive value indicates positive involvement.

Table 4 Y-randomization.

MODEL TYPE	R	R^2	Q^2LOO
Original	0.923968	0.853717	0.768629
Random 1	0.316429	0.100127	-0.5018
Random 2	0.480813	0.231181	-0.26962
Random 3	0.352661	0.124369	-0.60309
Random 4	0.511229	0.261355	-0.37775
Random 5	0.35575	0.126558	-0.77112
Random 6	0.407573	0.166115	-0.42048
Random 7	0.618144	0.382102	-0.57508
Random 8	0.322444	0.10397	-0.8701
Random 9	0.3577	0.127949	-0.56328
Random 10	0.354681	0.125799	-1.3774
Random Models Parameters			
Average R	0.454672		
Average R^2	0.236659		
Average Q^2(LOO)	-0.05055		
cRp^2	0.766093		

Table 5- Pearson's correlation matrix, VIF and Mean effect of the descriptors in model 5.

	AATS3i	VE3_Dze	SpMax2_Bhm	TopoPSA	E3s	VIF	ME
AATS3i	1					1.46933	0.50073
VE3_Dze	-0.1715	1				1.19188	0.00685
SpMax2_Bhm	-0.5069	0.123671	1			1.38420	0.51482
TopoPSA	0.04205	-0.07802	-0.10135	1		1.04016	-0.00804
E3s	0.39389	-0.40071	-0.32009	0.182022	1	1.43328	-0.01437

Figure 1 depicts a linear relationship between anticipated and observed activities, indicating the model's strength with regard to parameters. The plot of normalized residuals versus real residuals (Figure 2) shows a compound dispersion on both sides of zero, indicating that the model was constructed without systematic error. William's plot (Figure 3) revealed five influential compounds from the test set and one from the training set, each with leverage values above the threshold (h* = 0.82). This means the aforementioned compounds are beyond the application domain and must be removed while fresh piperidine-4-amine compounds are created.

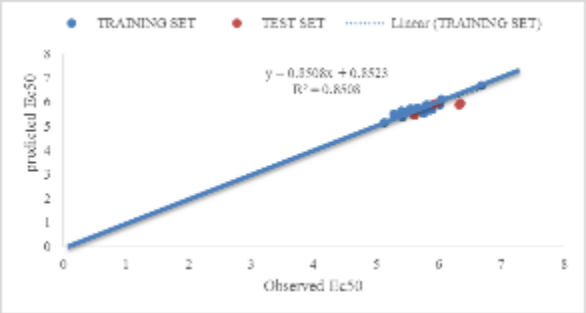


Figure 1. XY (Scatter) Plot of the actual pEC_{50} against predicted pEC_{50} of training set and test set of the selected model.



Figure 2. XY (Scatter) Plot of actual pEC_{50} against the residuals of both the test and training sets of the selected model.



Figure 3. Williams Plot of the selected model

DFT computations

To study the structure geometries, we did comprehensive geometry optimization for the analyzed compounds using DFT/B3LYP level calculations (Table 6). We achieved this by employing the frontier molecular orbital energies of a molecule that postulates how essential its properties are in terms of interactions involving charge transfer with other species (particularly in the active site of proteins/enzymes) and aids in understanding its stability. A compound's energy band gap (ΔE) determines its electrical and optical

characteristics, indicating its reactivity (Ibrahim *et al.*, 2024). The electron-rich nucleus (HOMO) can donate electrons, whereas the electron-deficient core (LUMO) can take electrons. Negative energy disparity (ΔE= LUMO-HOMO) values in the most successful compounds imply greater stability, which is crucial in the building of a very stable complex. In addition, a variance in energy is used to determine the most powerful compounds among the top hits. Electrons are donated by a compound's electron-rich nucleus (HOMO) and accepted by its electron-deficient core (LUMO) in drugs development. Successful compounds have a narrower energy gap (ΔE = LUMO-HOMO), which improves stability and makes it easier for HOMO and LUMO to transfer charges. This increases the target enzyme's affinity and bioactivity. Compounds having a wider energy gap, on the other hand, exhibit less bioactivity because charge transfer is impeded. With a low energy gap of 2.64 eV, compound 24, the most powerful hit, shows great promise for sustained interactions with the NS5B polymerase, indicating effectiveness in preventing the replication of the Hepatitis C virus (Ibrahim *et al.*, 2024). The most powerful hit, Compound 24, exhibits the lowest potential and lowest band/energy gap (ΔE) of 2.64 eV (Table 6). Therefore, it is regarded as the most responsive of those described (which may explain how it possesses the greatest affinity towards the NS5B polymerase enzyme due to the small band difference). Smaller gaps between bands suggest greater stability during complicated growth.

Furthermore, as the range separating HOMO and LUMO energies closes or expands, a compound's reactivity increases or decreases. Compound 24 (2.64eV) is the most reactive, followed by Compound 23 (3.05eV), Compound 25 (3.84eV), and Compound 6 (-3.91eV). The molecules' HOMO and LUMO energies were utilized to determine qualitative compound characteristics (η, δ, χ, μ, as well as ω) and verify their ability to react, stability, and optical features (refer to Table 6). Chemical hardness (η) relates to molecular durability and responsiveness. A harder structure possesses a greater band gap, which indicates that it is less susceptible to damage. A soft molecule has a smaller gap between bands. Figure 4 depicts the best compounds' frontier molecular orbital (FMO) (also known as HOMO and LUMO) energy maps.

Table 6- Frontier molecular-orbital energies and global-reactivity descriptors of the studied ligands.

S/N	EH	EL	DE	IP	EA	η	□	μ	ω
24	-5.66	-3.02	2.64	5.66	-3.02	4.15	7.17	-4.15	35.73669
23	-5.69	-2.64	3.05	5.69	-2.64	4.37	7.01	-4.37	41.72673
25	-5.73	-1.89	3.84	5.73	-1.89	4.78	6.675	-4.78	54.77922
6	-4.41	-0.50	3.91	4.41	-0.50	4.16	4.66	-4.16	35.99565
7	-4.59	-0.15	4.44	4.59	-0.15	4.51	4.65	-4.51	46.01965

The MEP surface map is a valuable tool for understanding how a molecule interacts with other molecules, especially with target enzymes NS5B polymerase. In the case of compound 24, red areas represent negative potential zones, while blue areas indicate positive potential zones. Positive potential regions on the compound can interact well with negative regions on the enzyme, potentially improving binding. Blue areas around compound 24's benzene groups suggest favorable interaction sites, while red regions on nitrogen and oxygen atoms indicate potential positive interactions. Analyzing these color-coded regions on the MEP surface map helps predict and interpret the compound's binding affinity and interactions with the enzyme on a molecular level. Figure 5 illustrates the MEPS maps for the best-hit compound 24. Colors represent the optical characteristics and intensity of the MEP surface for molecule 24. On the MEPS map, red indicates a negative potential zone/region, whereas blue indicates a positive potential zone/region. The blue-colored area, indicating the positive prospective zone, was most noticeable in compound 24's benzene groups. On the contrary, partially red colors represented the negative potential zone on the nitrogen and oxygen atoms of compound 24. In addition, the green color

tinge indicates that the region/zone of zero electrical potential is centered on the carbon atom.

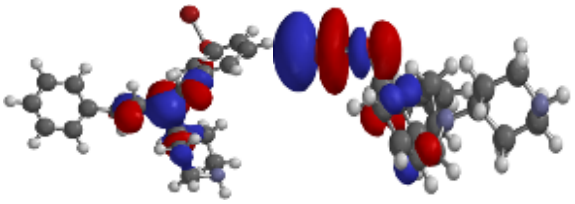


Figure 4. Shapes of MOs frontiers of compound 24 obtained by DFT (B3LYP/6-31G*) method

Docking results

A docking investigation were conducted among new piperidin-4-amine compounds and the downloadable NS5B polymerase receptor, protein data bank code 3FQK. Tables 7 exhibit the outcomes of interactions, known as MolDock scores. Docking experiments indicated significant docked compounds engage with receptors. We discovered a wide range of bonding interactions amongst the ligands, involving hydrophobic, electrostatic, amide, and conventional hydrogen bond interaction. According to the docking data provided in Table 7, compound 26 generated bonds and non-bond interactions at the receptors' (NS5B polymerase) binding pocket with the highest MolDock Score of -142.24 (kcal/mol), Rerank Score of -115.6, and post energy Score of -144.78 (kcal/mol), Compound 30 was placed second due to its mole dock score of -140.70 kcal/mol, then came compound 3 with a mole dock score of -135.70 kcal/mol then Molecule 21 with a mole dock score of -129.11 kcal/mol. Compound 26 showed superior binding interactions at the NS5B polymerase binding pocket compared to compound 58 in the study by Bello et al. 2018. Compound 26 achieved higher scores across various parameters - a MolDock Score of -142.24 kcal/mol, a Rerank Score of -115.6, and a post-energy Score of -144.78 kcal/mol, indicating strong affinity and stability within the binding pocket. This suggests that compound 26 has greater potential for interactions with the NS5B polymerase, making it a promising candidate for further development as a therapeutic agent for combating Hepatitis C.

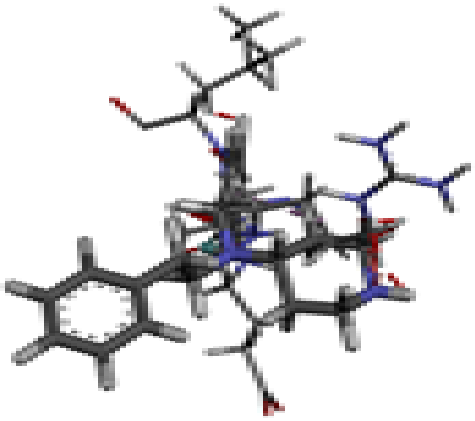
Table 7- MolDockScore, Plants Score, RerankScore of the piperidin-4-amine ligands.

Molecules	MolDock Score (kcal/mol)	Heavy Atoms	Pose Energy	RerankScore
molecule 1	-115.84	23	-102.84	-71.92
molecule 2	-111.00	24	-108.35	-86.28
molecule 3	-135.70	24	-133.66	-108.3
molecule 4	-124.31	24	-122.38	-97.30
molecule 5	-128.70	25	-123.43	-103.87
molecule 6	-116.79	23	-113.29	-63.75
molecule 7	-117.74	23	-114.90	-87.82
molecule 8	-108.06	22	-107.31	-75.82
molecule 9	-111.90	23	-107.89	-87.35
molecule 10	-113.01	23	-111.78	-18.16
molecule 11	-114.95	23	-112.51	-89.48
molecule 12	-126.47	26	-122.83	-82.80
molecule 13	-124.78	27	-122.79	-96.96
molecule 14	-117.04	24	-108.16	-86.65
molecule 15	-124.40	24	-119.43	-97.93
molecule 16	-114.92	24	-112.39	-87.05
molecule 17	-112.73	23	-109.48	-89.65
molecule 18	-115.23	23	-112.38	-65.50
molecule 19	-116.55	23	-114.77	-88.88
molecule 20	-123.86	26	-123.67	-84.24
molecule 21	-129.11	27	-124.47	-106.24
molecule 22	-112.98	23	-108.96	-66.91
molecule 23	-126.42	24	-128.60	-96.81
molecule 24	-126.23	24	-126.80	-97.43
molecule 25	-114.26	24	-105.98	-69.87
molecule 26	-142.24	27	-144.78	-115.6
molecule 27	-120.98	25	-124.96	-91.14

molecule 28	-120.10	24	-117.04	-95.98
molecule 29	-120.75	24	-119.02	-96.03
molecule 30	-140.70	24	-137.40	-110.79
molecule 31	-123.90	24	-111.40	-99.79
FDA Rib/Pig	-111.095	37	-97.670	-46.992

Compound 26, the top compound among the NS5B polymerase inhibitors under investigation, was found to have six different Forms of relationships with NS5B polymerase's active site. The observed interactions and bond angles were: Conventional Hydrogen Bond with SER470 at a distance of 2.79357 Å, Carbon Hydrogen Bond with ILE463, ARG465, and GLY468 at a distance of 2.55263 Å, 2.52434 Å, and 1.94861 Å, Halogen (Fluorine) Bond with GLU464, ARG465 at a distance of 3.20431 Å and 3.5447 Å, Hydrophobic Alkyl with ILE462, and LEU545, at a distance of 5.10295 Å and 5.42326 Å, and Hydrophobic Pi, Figure 6.

Compound 30, The second-greatest chemical in its category of piperidine-4-amine inhibitors under investigation, had connections and bond distance via 2 Carbon Hydrogen Bond of GLU464, ALA542 at a distance of 2.18454 Å and 2.60628 Å, 2 Halogen (Fluorine) connection between PRO460, GLN461 at a distance of 2.97536 Å and 3.44833 Å, and Hydrophobic Alkyl interaction ARG465, LEU466 and ILE462 at a distance of 3.74417 Å.



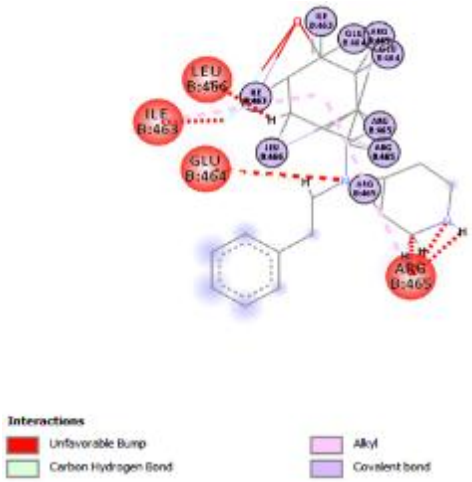


Figure 6- 2d, 3d view and hydrogen bond interaction of the componud 26 using dicovery studio virtualizer.



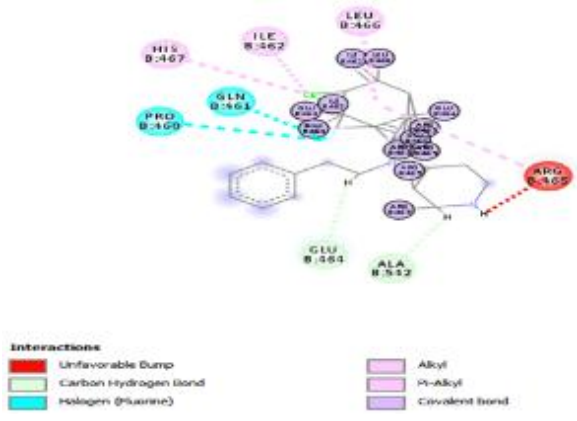


Figure 7- 2d, 3d view and hydrogen bond interaction of the componud 30 using dicovery studio virtualizer.

Assessing drug-likeness and ADMET characteristics

The SwissADME online tool was utilized to predict the drug-likeness properties of piperidine-4-amine compounds, as shown in Table 8. Drug-likeness characteristics constitute the primary parameters utilized to screen potential drugs early in the drug development stage. This approach can be characterized as a way to link a compound's physicochemical qualities to its biopharmaceutical aspect in the human system, specifically focusing on oral bioavailability. Lipinski's rule was utilized to assess drug-likeness qualities. It implies that effective consumption or penetration takes place when the molecular weight (MW) is below 500, the amount of hydrogen bond donors (HBDs) is lower than 5, the partition coefficient Log P is lower than 5, and the number of hydrogen bond acceptors (HBAs) is beneath ten (including all N and O atoms). As demonstrated in Table 8, all of the piperidine-4-amine derivatives satisfy Lipinski's criterion, indicating that these compounds possess the best oral bioavailability.

Table 8-Drug-like features of the analogues.

S/N	Molecule	MW	H-bond acceptors	H-bond donors	TPSA	iLOGP	Lipinski violations	Synthetic Accessibility
1	Molecule 1	314.51	2	1	15.27	3.98	0	3.12
2	Molecule 2	328.53	2	1	15.27	4.12	1	3.23
3	Molecule 3	320.47	1	1	15.27	3.78	0	2.80
4	Molecule 4	320.47	1	1	15.27	3.53	0	2.62
5	Molecule 5	336.47	2	1	32.34	3.23	0	2.55
6	Molecule 6	330.53	2	1	34.48	0.00	0	4.92
7	Molecule 7	330.53	1	1	34.48	0.00	0	4.52
8	Molecule 8	294.43	2	1	15.27	3.27	0	1.93
9	Molecule 9	328.88	2	1	15.27	3.8	0	2.12
10	Molecule 10	373.33	2	1	15.27	3.88	0	2.18
11	Molecule 11	312.41	3	1	15.27	3.61	0	2.13
12	Molecule 12	362.47	5	1	15.27	3.73	1	2.31
13	Molecule 13	378.47	6	1	24.50	3.74	0	2.39
14	Molecule 14	324.46	3	1	24.50	3.75	0	2.15
15	Molecule 15	324.46	3	1	24.50	3.75	0	2.15
16	Molecule 16	319.44	3	1	39.06	3.39	0	2.30
17	Molecule 17	328.88	2	1	15.27	3.77	0	2.21
18	Molecule 18	373.33	2	1	15.27	3.87	0	2.30
19	Molecule 19	312.41	3	1	15.27	3.63	0	2.16
20	Molecule 20	362.47	5	1	15.27	3.88	1	2.43
21	Molecule 21	378.47	6	1	24.50	3.68	0	2.49
22	Molecule 22	300.40	2	1	15.27	3.78	0	2.12
23	Molecule 23	348.48	3	1	24.50	3.84	0	2.19
24	Molecule 24	389.38	3	1	24.50	3.93	0	2.50
25	Molecule 25	328.41	4	1	24.50	3.78	0	2.56
26	Molecule 26	376.47	6	1	24.50	3.68	0	2.49
27	Molecule 27	340.47	4	1	33.73	3.90	0	2.85
28	Molecule 28	332.43	2	1	15.27	3.84	1	2.32
29	Molecule 29	402.77	2	1	15.27	4.01	1	2.47
30	Molecule 30	346.87	3	1	15.27	3.83	1	2.38
31	Molecule 31	362.47	3	1	15.27	3.79	1	2.33

The central nervous system (CNS) permeability is set at > -2 to -3, whereas the blood-brain barrier (BBB) permeability is set at > 0.3 to -1. It was observed that all of the top-hit compounds

exhibited 100% intestinal absorption in humans (HIA), indicating that these anti-hepatitis C inhibitors can be absorbed in the human gut. Furthermore, the HIA values were designed to exceed the 30% minimum proposed rate set for this property's appraisal. The BBB permeability of the hit compounds was revealed to be -1, indicating that the compounds had a limited potential to infiltrate or permeate the BBB. All chemicals have a CNS permeability value of -2, which means they can only enter or permeate the CNS in very small amounts. The drugs' ability to act as both CYP34A substrates and inhibitors in a proportionate manner indicates their metabolic properties. "Total clearance" refers to the relationship between a drug's rate of removal and its concentration in the body, which serves as an indicator.

Table 9- ADMET Properties of the best highest compounds.

S/N	GI Absorption	BBB permeant	Pgp substrate	Bioavailability score
Molecule 3	High	Yes	No	0.55
molecule 5	High	yes	No	0.55
molecule 21	High	Yes	No	0.55
molecule 26	High	Yes	No	0.55
molecule 30	High	Yes	No	0.55

Many potential drugs never reach clinical trials because to ADMET concerns. Because of its significance, ADMET qualities are currently being examined in the initial stages of pharmaceutical studies, leading to a substantial decrease in the number of compounds that failed in clinical studies because of inadequate ADMET features (Daina *et al.*, 2017). Table 9 lists some of the essential computed ADMET parameters, including human intestinal absorption (HIA), plasma glycoprotein (Pgp) inhibitor, plasma glycoprotein (Pgp) substrate, blood-brain barrier (BBB) penetration, and human cytochromes (CYP). The lead compounds' BBB permeated output was classed as BBB+, with anticipated values higher than -1. The anticipated metabolic outputs revealed the odds of being lead inhibitors or substrates of CYPs (1A2, 3A4, 2C9, 2C19, and 2D6) isoenzymes ranged from 0 to 1. A drug's clearance (CL) is another key pharmacokinetic parameter that explains how the medication is eliminated from the body. The lead compounds' clearance penetration levels are expected to be minimal. As a result, none of the chemicals presented any major toxicity profile hazards in terms of respiratory or toxicity.

Molecular docking of newly developed piperidin-4-amine inhibitors.

Following the DBVS (docking-based virtual screening) of the 31 piperidine-4-amine derivatives against the NS5B polymerase inhibitor, compound 26 via a mole dock score of -142.24 kcal/mol emerged as the most effective, top-ranked hit among the compounds being studied and proved thus retained as the template compound. Compound 26 was meant to be separated into two main components (R1 and R2). R1 is a benzene element whereby a long-chain hydrogen or fatty primary alcohol replaces the methyl on the nitrogen atom of the benzene moiety, revealing potential action sites involving mutant NS5B polymerase residues. While R2 is where side chains of various dimensions were inserted to find the best fit set, which can affect the inhibitory activity of the mutant NS5B polymerase. This technique resulted in the development of six novel compounds, including compound SDD5 and SDD6, which have a higher affinity than the template. Figure 8.

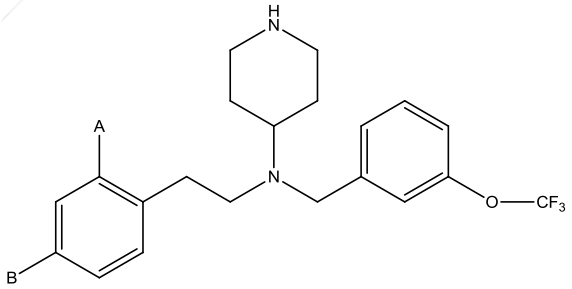


Figure 8 depicts the structural skeleton of compound 26 with A and B positions as points of connection.

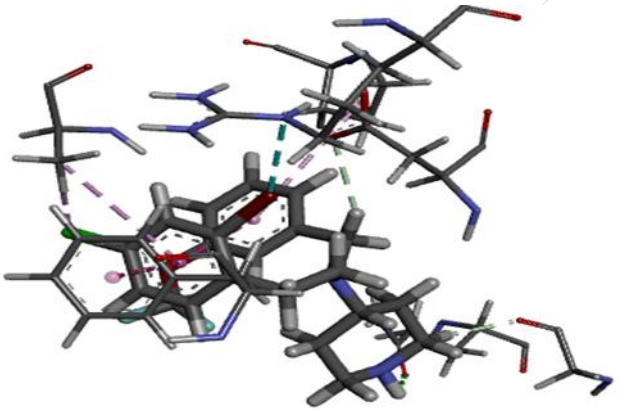
Molecular docking of newly developed molecules.

Piperidine-4-amine inhibitors to acquire clarity regarding the ligand-protein interactions, molecular docking was used between the newly developed piperidin-4-amine inhibitors and the target (NS5B polymerase). Table 10 displays the mole dock values for the newly developed piperidin-4-amine inhibitors, which ranged from -127.89 to -153.79 kcal/mol.

Table 10- shows the MolDockScore, Plants Score, and RerankScore for the newly designed compounds.

Name	MolDock Score (kcal/mol)	Heavy Atoms	PlantsScore (kcal/mol)	RerankScore
SDD1	-127.89	29	-121.31	-114.08
SDD2	-83.870	29	-77.740	-90.50
SDD3	-105.20	29	-78.120	-80.61
SDD4	-95.361	29	-80.400	-70.38
SDD5	-146.10	30	-125.99	-123.44
SDD6	-153.74	29	-126.08	-155.60

SDD6 possesses the greatest mole dock value of -153.79 kcal/mol, followed by SDD5 (-146.10 kcal/mol) and SDD1 (-127.89 kcal/mol). Compound SDD6's 4-methylpiperrizin-1-yl (hydrophobic tail portions) and pyrimidine-4-yl (central hetero aromatic system) moieties engage to Conventional Hydrogen Bonds GLN446, ASP559, and GLY449 at 2.90583 Å, 2.64299 Å, and 2.04295 Å, accordingly. The core hetero aromatic structure, as well as the chemical's hydrophobic head and tail parts, communicated via hydrophobic Pi-Pi. The amino acid residues are stacked with PHE162 (4.5858 Å), Hydrophobic Alkyl with ALA97 (3.33548 Å, 4.44393 Å), and Halogen (Cl, Br, I) ARG168 (3.05914 Å), respectively. Fig



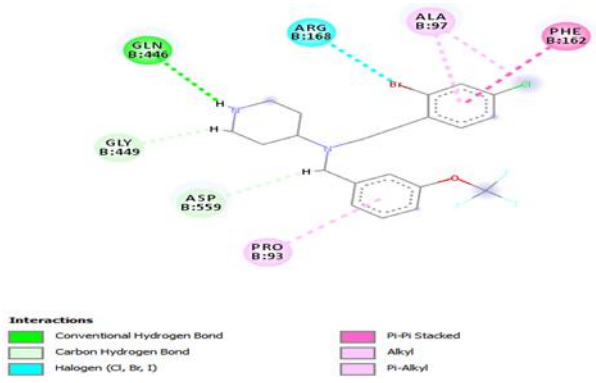


Figure 9 depicts the optimum SDD6 design in 2D and 3D views, as well as hydrogen bond interactions, using the Discovery Studio virtualizer.

Figure 10 demonstrates how the pyrimidine-4-yl moiety at the compound SDD5's central hetero aromatic system interacts with amino acids, SDD5 is the second-greatest developed compound which developed a hydrogen binding force with Pi-Donor Hydrogen Bond ASN142, 3.33263 Å, and then hydrophobic binding interaction with Hydrophobic Pi-Pi Stacked.

ADMET and drug-likeness properties of newly designed piperidin-4-amine inhibitors

Table 9A-The ADMET and drug-likeness properties of newly design compound.

Molecule	MW	nHBA	nHBD	GI absorption	BBB permeant	Pgp substrate	Lipinski violations	Bioavailability Score	Synthetic Accessibility
SDD1	491.7	6	1	Low	No	No	0	0.55	2.83
SDD2	430.8	7	1	High	No	No	0	0.55	2.83
SDD3	475.3	7	1	Low	No	No	0	0.55	2.81
SDD4	483.2	6	1	Low	No	Yes	0	0.17	2.89
SDD5	438.7	6	1	High	No	Yes	0	0.17	3.00
SDD6	409.7	7	1	Low	No	Yes	0	0.17	3.05

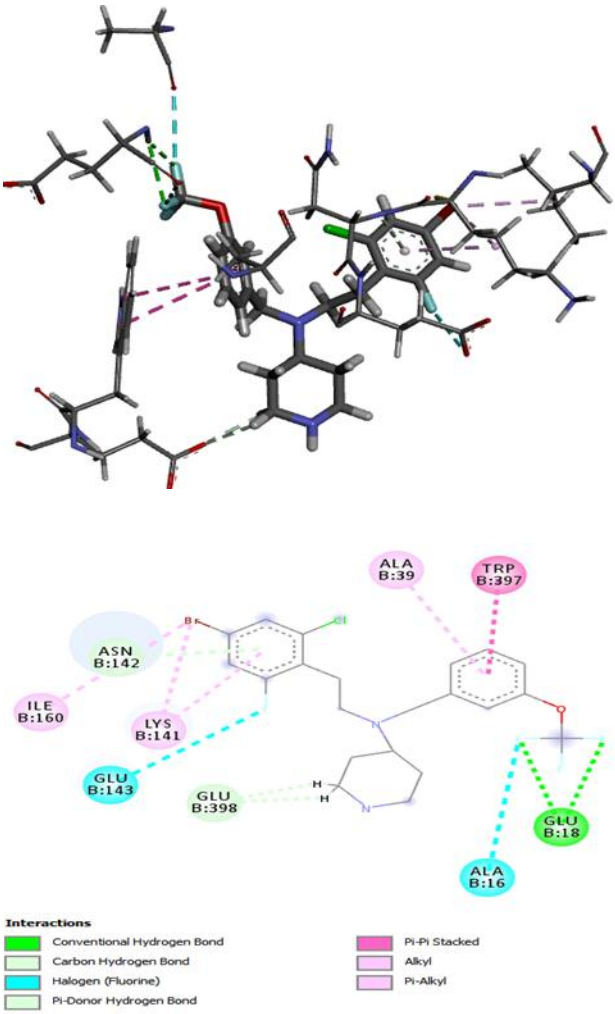


Figure 11. 2d, 3d view and hydrogen bond interaction of the best SDD5 design using dicovery studio virtualizer.

Lipinski's Rule of Five was used to predict the drug-like properties of the produced compounds. Each of the recently discovered compounds met Lipinski's rule of five (WM >500). Each had less than five and ten hydrogen bond donors and acceptors. These newly developed compounds had a synthetic accessibility score of <5. This means that the freshly identified chemicals possess an excellent potential of being easily produced in the laboratory. Based on this, the recently identified compounds are likely to be drug-like, orally accessible, and efficacious. Table 9A depicts the expected ADMET properties of these newly synthesized compounds. The intestinal absorption values for these newly discovered compounds were all greater than 90 percent and lower than 100. Their intestinal absorption rates exceeded the 30% threshold, demonstrating that the freshly developed compounds exhibit excellent human intestine absorption properties. Freshly synthesized drugs have BBB permeability (log BB) values of < -1, indicating inadequate dispersion across the brain. All CNS permeability (Log PS) values were larger than -2, indicating CNS penetration. Furthermore, compounds were revealed to serve as simultaneous substrates and inhibitors of CYP3A4, corroborating similar metabolic characteristics. Additionally, the overall clearance of a medication molecule in the body for these newly created compounds was satisfactory. Most of the recently created chemicals are harmless. According to these estimated characteristics, the newly created compounds ought to possess an elevated absorption value, low toxicity, and good permeability across the cell membrane. Ultimately, all of the recently discovered medicines were expected to possess acceptable pharmacokinetic properties.

Conclusion

In this study, genetic function algorithms were employed to do quantitative structure-activity relationship modeling to forecast new inhibitory actions of piperidin compounds as anti-Hepatitis C drugs. The equilibrium structures for these anti-hepatitis C drugs were determined using a density functional theory technique at the B3LYP/6-31G* level of theory. The regression coefficients of the developed QSAR model revealed an equally good model with sufficient statistical validation keys R^2trng = 0.8537, R^2 adj = 0.8171, Q^2cv = 0.7686, R^2test = 0.6979, and LOF (95%) = 0.1058 for the internal and external validations, which meets the criteria of acceptable QSAR models suggested by various groups. The proposed model's predictability, dependability, and robustness were proven by the applicability domain and Y-scrambling tests. Compound 26 was chosen since it has the highest MolDock score of -142.24, Plant Score of -144.78, and Rerank Score of -115.6 kcal/mol among co-ligands, and it is easy to modify around its benzene ring moiety to build novel compounds. The ADME characteristics and drug-likeness of the identified Piperidin compounds were predicted using the pharmacokinetic profiles of these compounds and SWISS ADME. These compounds were discovered to violate not more than the minimum requirements established by Lipinski's rule of five. SAD6, with the highest MolDock

score of -153.74, Plant Score of -126.08, and Rerank Score of -155.60 kcal/mol, was found to be more potent compared to the template and the FDA-approved medicine for Hepatitis C due to the inclusion of the new substituent. The ADME properties and drug-likeness of the recently developed molecules show that not violate more than one of the criteria listed in Lipinski's rule of five, implying that all of these molecules have a high probability of being pharmacologically active. Compounds can be produced in the laboratory by their synthetic accessibility score. The findings of this study pave the path for the creation of new, potent anti-hepatitis C inhibitors directed at their target enzyme.

Acknowledgements

Funding

"This research did not receive any specific grant from funding agencies in the public, commercial or not-for-profit sectors"

Competing interests

The authors declare that they have no competing interests.

Compliance with ethics requirement

Not applicable.

References

Abdulfatai, U., Uzairu, A., and Uba, S. (2017). Quantitative structure-activity relationship and molecular docking studies of a series of quinazolinonyl analogues as inhibitors of gamma amino butyric acid aminotransferase, Journal of advanced research, 8(1), 33-43.

Abdullahi, M., Uzairu, A., Shallangwa, G. A., Arthur, D. E., Umar, B. A., and Ibrahim, M. T. (2020). Virtual molecular docking study of some novel carboxamide series as new anti-tubercular agents, European Journal of Chemistry, 11(1), 30-36.

Aouidate, A., Ghaleb, A., Ghamali, M., Chtita, S., Ousaa, A., Sbai, A., et al. (2018). Molecular docking and 3D-QSAR studies on 7-azaindole derivatives as inhibitors of Trk a: a strategic design in novel anticancer agents, Letters in Drug Design & Discovery, 15(11), 1211-1223.

Baldi, A. (2010). Computational approaches for drug design and discovery: An overview, Systematic reviews in Pharmacy, 1(1), 99.

Baumert, T. F., and Hoshida, Y. (2019). Addressing the challenges of hepatitis C cure and persistent risk of hepatocellular carcinoma (Vol. 11, pp. 441): MDPI.

Bello, A. S., Uzairu, A., Shallangwa, G. A., Ibrahim, A., & Ibrahim, M. T. (2024). Computer-aided molecular modeling and design studies of some N-(4-(dimethyl amino) phenyl)-4-methoxy-3-propionamidobenzamide derivatives as NS5B polymerase inhibitors. The Microbe, 4, 100154.

Bollag, G., Hirth, P., Tsai, J., Zhang, J., Ibrahim, P. N., Cho, H., et al. (2010). Clinical efficacy of a RAF inhibitor needs broad target blockade in BRAF-mutant melanoma, Nature, 467(7315), 596-599.

Chtita, S., Ghamali, M., Larif, M., Adad, A., Hmammouchi, R., Bouachrine, M., et al. (2013). Prediction of biological activity of imidazo [1, 2-a] pyrazine derivatives by combining DFT and QSAR results, International Journal of Innovative Research in Science, Engineering and Technology, 2(11), 7951-7962.

Cui, W., Aouidate, A., Wang, S., Yu, Q., Li, Y., and Yuan, S. (2020). Discovering anti-cancer drugs via computational methods, Frontiers in Pharmacology, 11, 733.

Daina, A., Michielin, O., and Zoete, V. (2017). SwissADME: a free web tool to evaluate pharmacokinetics, drug-likeness and medicinal chemistry friendliness of small molecules, Scientific reports, 7(1), 1-13.

Di, L., Artursson, P., Avdeef, A., Benet, L. Z., Houston, J. B., Kansy, M., et al. (2020). The critical role of passive permeability in designing successful drugs, ChemMedChem, 15(20), 1862-1874.

El Kalai, F., Chelfi, T., Benchat, N., Hacht, B., Bouklah, M., Elaatiaoui, A., et al. (2019). New organic extractant based on pyridazinone scaffold compounds: Liquid-liquid extraction study and DFT calculations, Journal of Molecular Structure, 1191, 24-31.

Fadl, N., and Salem, T. Z. (2020). Hepatitis C genotype 4: A report on resistance-associated substitutions in NS3, NS5A, and NS5B genes, Reviews in Medical Virology, 30(4), e2120.

Fukui, K. (1982). Role of frontier orbitals in chemical reactions, Science, 218(4574), 747-754.

Gázquez, J. L. (1993). Hardness and softness in density functional theory, Chemical hardness, 27-43.

Hadaji, E. G., Bourass, M., Ouammou, A., and Bouachrine, M. (2017). 3D-QSAR models to predict anti-cancer activity on a series of protein P38 MAP kinase inhibitors, Journal of Taibah University for Science, 11(3), 392-407.

Hamdane, N., Jühling, F., Crouchet, E., El Saghire, H., Thumann, C., Oudot, M. A., et al. (2019). HCV-induced epigenetic changes associated with liver cancer risk persist after sustained virologic response, Gastroenterology, 156(8), 2313-2329. e2317.

Ibrahim, M. T., Tabti, K., Abdulsalam, S., Tahir, A. S., Mahmoud, A., and Danmallam, A. M. (2024). Discovery of new 2, 4-diaminopyrimidines derivatives as EGFRT790M kinase inhibitors: a structure-based approach with DFT calculation, drug-likeness, ADME-toxicity properties evaluation and MD simulation, Journal of Umm Al-Qura University for Applied Sciences, 1-17.

Ibrahim, M. T., Uzairu, A., Shallangwa, G. A., and Uba, S. (2020a). Computer-aided molecular modeling studies of some 2, 3-dihydro-[1, 4] dioxino [2, 3-f] quinazoline derivatives as EGFRWT inhibitors, Beni-Suef University Journal of Basic and Applied Sciences, 9(1), 1-10.

Ibrahim, M. T., Uzairu, A., Shallangwa, G. A., and Uba, S. (2020b). Structure-based design and activity modeling of novel epidermal growth factor receptor kinase inhibitors; an in silico approach, Scientific African, 9, e00503.

Ibrahim, M. T., Uzairu, A., Uba, S., and Shallangwa, G. A. (2020). Quantitative structure-activity relationship, molecular docking, drug-likeness, and pharmacokinetic studies of some non-small cell lung cancer therapeutic agents, Beni-Suef University Journal of Basic and Applied Sciences, 9, 1-14.

Ismail, S. Y., and Uzairu, A. (2019). In silico QSAR and molecular docking studies of sulfur containing shikonin oxime derivatives as anti-cancer agent for colon cancer, Radiology of Infectious Diseases, 6(3), 108-121.

Kennedy, T. (1997). Managing the drug discovery/development interface, Drug discovery today, 2(10), 436-444.

Lee, C., Yang, W., and Parr, R. G. (1988). Development of the Colle-Salvetti correlation-energy formula into a functional of the electron density, Physical review B, 37(2), 785.

Molina–Infante, J., Romano, M., Fernandez–Bermejo, M., Federico, A., Gravina, A. G., Pozzati, L., et al. (2013). Optimized nonbismuth quadruple therapies cure most patients with Helicobacter pylori infection in populations with high rates of antibiotic resistance, Gastroenterology, 145(1), 121-128. e121.

Muhammad, U., Uzairu, A., and Ebuka Arthur, D. (2018). Review on: quantitative structure activity relationship (QSAR) modeling, J Anal Pharm Res, 7(2), 240-242.

Nilsson, M., Belfrage, A. K., Lindström, S., Wähling, H., Lindquist, C., Ayesa, S., et al. (2010). Synthesis and SAR of potent inhibitors of the hepatitis C virus NS3/4A protease: exploration of P2 quinazoline substituents, Bioorganic & medicinal chemistry letters, 20(14), 4004-4011.

Nulamuga, B., Uzairu, A., Babalola, I. T., Ibrahim, M. T., and Umar, A. B. (2023). In silico analysis of noscapine compounds as anti-tumor agents targeting the tubulin receptor, Journal of Taibah University Medical Sciences, 18(1), 32.

Olasupo, S. B., Uzairu, A., Shallangwa, G., and Uba, S. (2019). QSAR analysis and molecular docking simulation of norepinephrine transporter (NET) inhibitors as anti-psychotic therapeutic agents, Heliyon, 5(10).

Pawlotsky, J.-M. (2016). Hepatitis C virus resistance to direct-acting antiviral drugs in interferon-free regimens, Gastroenterology, 151(1), 70-86.

Perez, S., Kaspi, A., Domovitz, T., Davidovich, A., Lavi-Itzkovitz, A., Meirson, T., et al. (2019). Hepatitis C virus leaves an epigenetic signature post cure of infection by direct-acting antivirals, PLoS genetics, 15(6), e1008181.

Qin, Q., Guo, Z., Lu, S., Wang, X., Fu, Q., Wu, T., et al. (2024). Discovery of novel 3-(1H-pyrazol-4-yl)-1H-indazole derivatives as potent type II TRK inhibitors against acquired resistance, European journal of medicinal chemistry, 264, 115953.

Rolt, A., Talley, D. C., Park, S. B., Hu, Z., Dulcey, A., Ma, C., et al. (2021). Discovery and optimization of a 4-aminopiperidine scaffold for inhibition of hepatitis C virus assembly, Journal of medicinal chemistry, 64(13), 9431-9443.

Shaw, J., Gosain, R., Kalita, M. M., Foster, T. L., Kankanala, J., Mahato, D. R., et al. (2020). Rationally derived inhibitors of hepatitis C virus (HCV) p7 channel activity reveal prospect for bimodal antiviral therapy, Elife, 9, e52555.

Thomsen, R., and Christensen, M. H. (2006). MolDock: a new technique for high-accuracy molecular docking, Journal of medicinal chemistry, 49(11), 3315-3321.

Umar, A. B., Uzairu, A., Shallangwa, G. A., and Uba, S. (2021). Ligand-based drug design and molecular docking simulation studies of some novel anticancer compounds on MALME-3M melanoma cell line, Egyptian Journal of Medical Human Genetics, 22(1), 1-15.

Wolinski, K., Hinton, J. F., and Pulay, P. (1990). Efficient implementation of the gauge-independent atomic orbital method for NMR chemical shift calculations, Journal of the American Chemical Society, 112(23), 8251-8260.

Yap, C. W. (2011). PaDEL-descriptor: An open source software to calculate molecular descriptors and fingerprints, Journal of computational chemistry, 32(7), 1466-1474.

Abdullahi, M., Uzairu, A., Shallangwa, G. A., Arthur, D. E., Umar, B. A., and Ibrahim, M. T. (2020). Virtual molecular docking study of some novel carboxamide series as new anti-tubercular agents, *European Journal of Chemistry*, ***11***(**1**), **30-36** .

Bello, A. S ,.Uzairu, A., Shallangwa, G., and Ibrahim, M. T. (2024). COMPUTER-AIDED MOLECULAR MODELING AND DESIGN STUDIES OF SOME N-(4-(DIMETHYL AMINO) PHENYL)-4-METHOXY-3-PROPIONAMIDOBENZAMIDE DERIVATIVES AS NS5B POLYMERASE INHIBITORS, *The Microbe*, **100154** .

Cui, W ,.Aouidate, A., Wang, S., Yu, Q., Li, Y., and Yuan, S. (2020). Discovering anti-cancer drugs via computational methods, *Frontiers in Pharmacology*, ***11***, **733** .

Daina, A., Michielin, O., and Zoete, V. (2017). SwissADME: a free web tool to evaluate pharmacokinetics, drug-likeness and medicinal chemistry friendliness of small molecules, *Scientific reports*, ***7***(**1**), **1-13** .

El Kalai, F., Chelfi, T., Benchat, N., Hacht, B., Bouklah, M., Elaatiaoui, A., et al. (2019). New organic extractant based on pyridazinone scaffold compounds: Liquid-liquid extraction study and DFT calculations, *Journal of Molecular Structure*, ***1191***, **24-31** .

Fukui, K. (1982). Role of frontier orbitals in chemical reactions, *Science*, ***218***(**4574**), **747-754** .

Gázquez, J. L. (1993). Hardness and softness in density functional theory, *Chemical hardness*, **27-43** .

Ibrahim, M. T., Tabti, K., Abdulsalam, S., Tahir, A. S., Mahmoud, A., and Danmallam, A. M. (2024). Discovery of new 2, 4-diaminopyrimidines derivatives as EGFRT790M kinase inhibitors: a structure-based approach with DFT calculation, drug-likeness, ADME-toxicity properties evaluation and MD simulation, *Journal of Umm Al-Qura University for Applied Sciences*, **1-17** .

Ismail, S. Y., and Uzairu, A. (2019). In silico QSAR and molecular docking studies of sulfur containing shikonin oxime derivatives as anti-cancer agent for colon cancer, *Radiology of Infectious Diseases*, ***6***(**3**), **108-121** .

Muhammad, U., Uzairu, A., and Ebuka Arthur, D. (2018). Review on: quantitative structure activity relationship (QSAR) modeling, *J Anal Pharm Res*, ***7***(**2**), **240-242** .

Nulamuga, B., Uzairu, A., Babalola, I. T., Ibrahim, M. T., and Umar, A. B. (2023). In silico analysis of noscapine compounds as anti-tumor agents targeting the tubulin receptor, *Journal of Taibah University Medical Sciences*, ***18***(**1**), **32** .

Olasupo, S. B., Uzairu, A., Shallangwa, G., and Uba, S. (2019). QSAR analysis and molecular docking simulation of norepinephrine transporter (NET) inhibitors as anti-psychotic therapeutic agents, *Heliyon*, ***5*** .(١٠)

Thomsen, R ,.and Christensen, M. H. (2006). MolDock: a new technique for high-accuracy molecular docking, *Journal of medicinal chemistry*, ***49***(**11**), **3315-3321** .

Wolinski, K., Hinton, J. F., and Pulay, P. (1990). Efficient implementation of the gauge-independent atomic orbital method for NMR chemical shift calculations, *Journal of the American Chemical Society*, ***112***(**23**), **8251-8260** .